Journal of Computational Physics **178,** 520–532 (2002)
doi:10.1006/jcph.2002.7039, available online at http://www.idealibrary.com on IDEAL®

Nearest-Grid-Point Interpolation in Gyrokinetic Particle-in-Cell Simulation

Scott E. Parker

Center for Integrated Plasma Studies, Department of Physics, University of Colorado, Boulder, Colorado 80309

Received June 29, 2001; revised February 13, 2002

Linear interpolation or other higher order interpolation schemes are almost always used in particle-in-cell simulation because of their lower noise characteristics and accuracy relative to the nearest-grid-point method. The higher order interpolation schemes are chosen because of their optimal performance, balancing a smaller number of particles against more computer operations per particle per time step. However, this is *not* the case in large-scale gyrokinetic particle simulations, where sometimes nearest-grid-point interpolation is used with results virtually identical to those of linear interpolation using the same number of particles. Here, a comparison and analysis of nearest-grid-point and linear interpolation schemes is given showing why nearest-grid-point interpolation can be optimal. A simple two-dimensional slab model of the ion-temperature-gradient instability and associated generation of zonal flows is used to compare the interpolation schemes. Significant improvements in performance are possible by using nearest-grid-point interpolation because of the large number of gathers/scatters associated with gyroaveraging.

1. INTRODUCTION

There has recently been significant progress in kinetic simulation of turbulent energy transport in tokamak plasmas [1–5]. This progress has been due in part to the development of the gyrokinetic particle simulation method [6, 7] and δf methods [8–10], and to the enormous growth in the power of massively parallel computers. In Lee's seminal work on gyrokinetic particle simulation [7], he showed that only gyroaveraging over four points (the so-called four-point gyroaverage) was a reasonable approximation for $k_\perp \rho_i \lesssim 1 - 2$. This is important for computational efficiency because particle-in-cell (PIC) performance is closely tied to gather/scatter operations and each point in the gyroaverage involves such operations. In addition, spectral evaluation of the Bessel functions in the gyrokinetic formalism is impractical because a Fourier sum would be required for each particle for each time step. At first, it was surprising that the four-point gyroaverage was so accurate, but it has been well tested by Lee [7]. There is yet another surprise which vastly improves the performance

0021-9991/02 $35.00

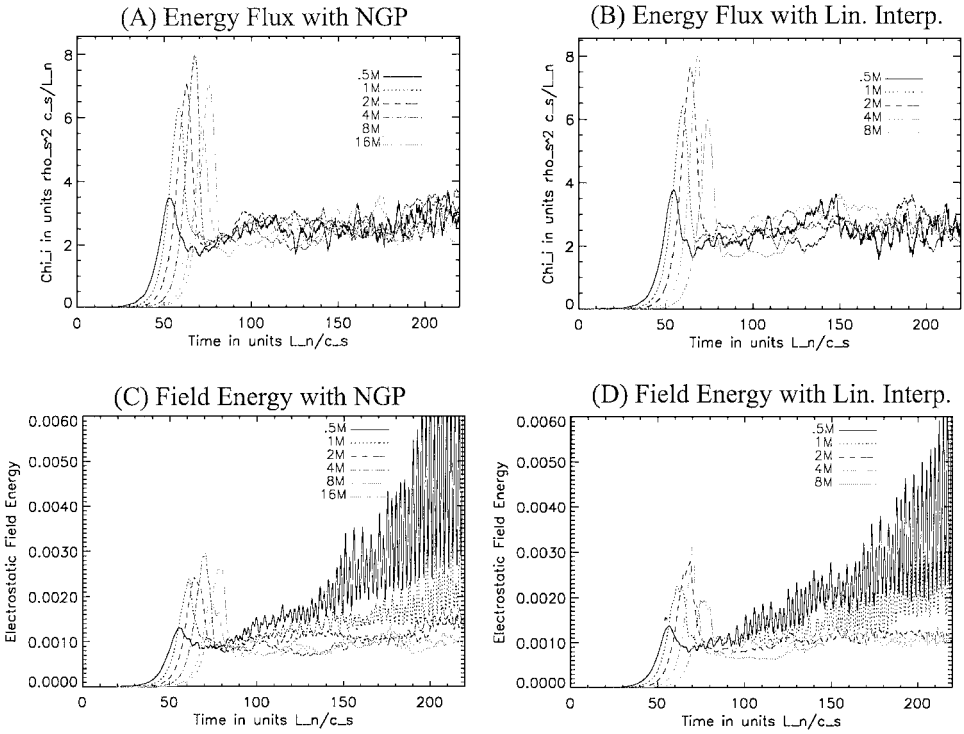

FIG. 1. Particle number convergence of the ion heat diffusivity and electrostatic field energy using both nearest grid point and interpolation in a three-dimensional toroidal flux-tube gyrokinetic turbulence simulation. Figures reprinted from Ref. [14].

of gyrokinetic simulations. That is, nearest-grid-point (NGP) interpolation introduces little noise and appears to be as accurate as higher order interpolation schemes, such as linear interpolation and the subtracted dipole approximation [11–13]. By this we mean that NGP simulations converge with respect to particle number as quickly as linear interpolation simulations. In addition, the results of the two interpolation methods are often nearly identical. This fact is part of the "art" of particle simulation and has not been well explained. However, recent large-scale simulations have used NGP [1, 2, 14]. Figures 1A–1D are reprinted from Ref. [14] and show comparison between NGP and linear interpolation in a three-dimensional toroidal flux-tube gyrokinetic turbulence simulation. Figure 1 shows that NGP and linear interpolation appear to produce similar results at moderate particle number (parameters and further details are given in Ref. [14]). The simulations from Fig. 1 showed that NGP interpolation performed approximately twice as fast as linear interpolation. Here, we study and explain why NGP works so well in gyrokinetic particle simulations. We find that the gyroaveraging acts as a further interpolation, averaging over nearby grid cells. Therefore, the underlying interpolation scheme (whether NGP, linear interpolation, or multipole) is in effect masked and is much less important than in conventional particle simulation using the Lorentz force. In this paper we only address why NGP and linear interpolation give similar results for gyrokinetic PIC simulations. All simulation results presented come from gyrokinetic simulations. We begin by discussing a simple two-dimensional bounded slab simulation model of zonal flow generation for the ion-temperature-gradient (ITG) instability. We use this model to test NGP and linear interpolation. Zonal flow generation is

an important saturation mechanism in ITG turbulence simulations and is a current area of research [15–17]. Next, a discussion of the effect of the interpolation methods is given. The gyroaveraging and interpolation are analyzed using particle shape functions [11, 13]. Finally, convergence with respect to particle number is discussed.

2. MODEL EQUATIONS

We begin by briefly mentioning the model equations used in the simulations presented in Section 3. This model is also used as a starting point to understand finite particle size effects in Section 4. For simplicity we restrict our discussion here to slab equations. A two-dimensional bounded slab model without magnetic shear is discussed further in Section 3 and used to simulate the generation of zonal flows. The ions are gyrokinetic and evolved using the δf method. This model has been discussed extensively in the literature and can be found in Refs. [1–4, 6–10, 14]. The ion gyrokinetic equation is

$$\partial_t \delta f + v_{||} \cdot \nabla_{||} \delta f + \mathbf{v}_E \cdot \nabla \delta f = -\left[\kappa_n + \frac{\kappa_T}{2}\left(v^2 - \frac{3}{2}\right)\right] \partial_y \phi f_M + v_{\parallel} \nabla_{\parallel} \phi f_M, \qquad (1)$$

where $\delta f(\mathbf{R}, v_{\parallel}, \mu)$ is the perturbed guiding center distribution function, $v_{||}$ is the velocity along the magnetic field line, $\mu = \frac{m v_{\perp}^2}{2B}$ is the magnetic moment, and $\mathbf{v}_E = \hat{b} \times \nabla \phi$. The following dimensionless units are used: $\mathbf{R} \to \mathbf{R}/\rho$, $t \to \Omega_i t$, $v_{||} \to v_{||}/v_{ti}$, and $\phi \to \frac{e\phi}{T_i}$. f_M is a Maxwellian distribution, $\kappa_n = |\partial_x n_0(x)/n_0|^{-1}$, and $\kappa_T = |\partial_x T_{i0}(x)/T_{i0}|^{-1}$. $\Omega_i = eB/(m_i c)$, $v_{ti} = \sqrt{T_i/m_i}$, and $\rho = v_{ti}/\Omega_i$ are the ion gyrofrequency, thermal speed, and gyroradius, respectively. In electrostatic gyrokinetic simulation, the field is solved for using quasineutrality and is algorithmically equivalent to solving the electrostatic Poisson's equation. The gyrokinetic quasineutrality condition is [6]

$$-\left(\frac{T_i}{T_e}\right)[1 - \Gamma_0(k_{\perp}^2)\phi(\mathbf{k})] = -[\delta \bar{n}_i(\mathbf{k}) - \delta n_e(\mathbf{k})], \qquad (2)$$

where $\delta n = (n - n_0)/n_0$ is the perturbed part of the density, $\delta \bar{n}_i$ is the perturbed gyrophase averaged ion density, and Γ_0 comes from gyroaveraging the Bessel function J_0. The appearance of the Γ_0 accounts for finite gyroradius effects. For small $k_{\perp}^2$, $1 - \Gamma_0(k_{\perp}^2)$ reduces to $k_{\perp}^2$.

For simplicity, we restrict our discussion here to an electrostatic adiabatic electron model, though these ideas could easily be generalized. Since the focus of this paper is on how NGP can be used when gyroaveraging the ions, the electron model is not crucial. For kinetic electrons, drift kinetic equations are used, so there is no gyroaveraging and linear interpolation would be a more appropriate choice. However, most large-scale simulations have been done using the adiabatic electron assumption [1–4]. To properly treat the adiabatic electron response, we must take the perturbed electron density to be of the form

$$\delta n_e = e[\phi - \langle \phi \rangle]/T_e, \qquad (3)$$

where T_e is the electron temperature and $\langle \phi \rangle$ denotes the purely radial (or flux surface average) electrostatic potential [18–20]. In this two-dimensional slab model the corresponding radial coordinate is x.

3. TWO-DIMENSIONAL SIMULATIONS OF ZONAL FLOW GENERATION

We now describe a very simple two-dimensional slab model without magnetic shear which is a minimal model for nonlinear saturation of the ITG instability [21, 22]. Here, we keep the evolution of the purely radial modes, which was not done in earlier simulations of this type [21–23]. This model shows the generation and saturation of zonal flow modes in a very simple system. Zonal flows have been found to be extremely important in determining the nonlinear saturation level and heat flux in three-dimensional toroidal gyrokinetic simulations [16–20, 24]. The limitation of the model presented here is that the final state is coherent whereas the toroidal simulations show a more turbulent state. However, coherent zonal flow modes have been shown to exist in small plasma volumes or situations with large amounts of profile variation [4, 25, 26].

We solve Eqs. (1)–(3) using the nonlinear δf PIC method [9]. In this two-dimensional slab model Eq. (3) simply reduces to $\delta n_e(k_y = 0) = 0$ and $\delta n_e = e\phi/T_i$ for all other k_y. The system is taken to be bounded in x so that $\phi(x = 0) = 0$ and $\phi(x = L_x) = 0$, where L_x and L_y are the size of the simulation domain in x and y, respectively (in the dimensionless units above). The model assumes uniformity in z, and a uniform magnetic field with a slight tilt in y [21], so that the direction of the B-field is $\hat{b} = \hat{z} + \theta\hat{y}$, assuming $\theta \ll 1$. This introduces as small but finite $k_{||}$, where $k_{||} \equiv \theta k_y$, which in turn introduces ion Landau damping, which is an essential ingredient of the ITG instability. This type of model has been used widely [21] and allows for modeling quasi-three-dimensional effects in a two-dimensional simulation.

The simulation uses a 16×16 grid with $\Delta x = \Delta y = \rho$. The results shown in Figs. 2–4 have 128 particles per grid cell. $\Omega_i \Delta t = 8.0$, $\theta = 0.01$, $T_i = T_e$, $\kappa_n = 0$, and $\kappa_T = 0.05$. The simulation has been linearly benchmarked with the results of Ref. [22]. The most unstable mode is (1, 1), $l = 1, m = 1$, where $k_x = \pi l/L_x$ and $k_y = 2\pi m/L_x$. The (1, 1) mode couples to the (1, −1) mode to produce a (2, 0) mode in the fashion

$$\phi(1, 1) + \phi(1, -1) \rightarrow \delta T(2, 0), \tag{4}$$

where $\delta T(2, 0)$ corresponds to a flattening of the profile (see Refs. [21, 22] for details on the mode-coupling theory). However, the generation of the purely radial $\delta T(2, 0)$ mode generates a corresponding purely radial electric field [26]

$$\phi(2, 0) \approx -\frac{1}{2}\left(1 + \frac{k_\perp^2}{k_x^2}\right)\delta T(2, 0), \tag{5}$$

where k_x is the radial wave number of $\phi(2, 0)$ and $k_\perp$ is that of the (1, 1) mode [26]. This $\phi(2, 0)$ mode can be thought of as the zonal flow of this simple model. The corresponding purely radial electric field generates a $E \times B$ shear flow in the y direction, which is stabilizing. In the more complex, three-dimensional flux-tube simulations this zonal flow is the dominant saturation mechanism.

Figure 2A shows the time evolution of the $\phi(1, 1)$ mode (real, imaginary parts and absolute value) using linear interpolation. The dark solid line is magnitude, the lighter line is the real part, and the lightest line is the imaginary part. Figure 2B shows the corresponding nonlinear energy flux. Figure 3A is the electrostatic potential as a function of x and y after saturation, showing that the $\phi(2, 0)$ zonal flow mode is dominant. Figure 3A shows the time history of this dominant zonal flow mode, $\phi(2, 0)$. Figures 2 and 3 are the results from linear interpolation. Figure 4 shows the corresponding time evolution of $\phi(1, 1)$ and the

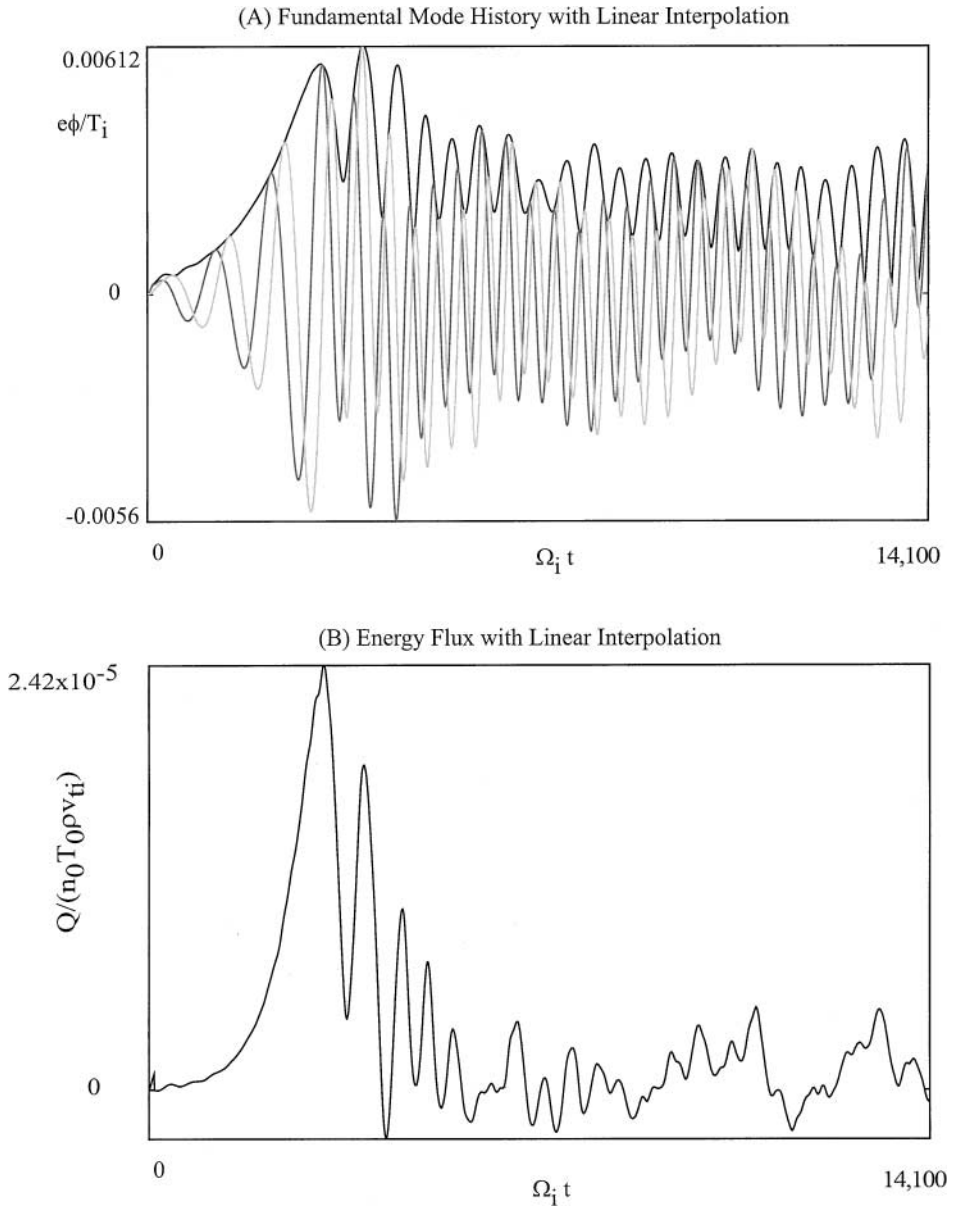

FIG. 2. Results using linear interpolation. (A) Time evolution of the most unstable mode, $\phi(k_x = \pi/L_x, k_y = 2\pi/L_y)$ (real, imaginary parts, and absolute value). The dark solid line is the magnitude, the lighter line is the real part, and the lightest line is the imaginary part. (B) The nonlinear ion energy flux.

heat flux using NGP interpolation showing that there is little difference between NGP and linear interpolation (Fig. 2).

It has been found that without the zonal flow generation, the nonlinear saturation is due primarily to wave-particle trapping, and that the saturation level can be estimated by balancing the growth rate with the trapping frequency [22], producing $|\phi| = \frac{1}{2}\frac{\gamma}{k_x k_y}$ using the dimensionless units discussed above. This estimate for the saturation level gives 0.63%, which compares well with the 0.61% shown in Fig. 2A. However, we expect this estimate

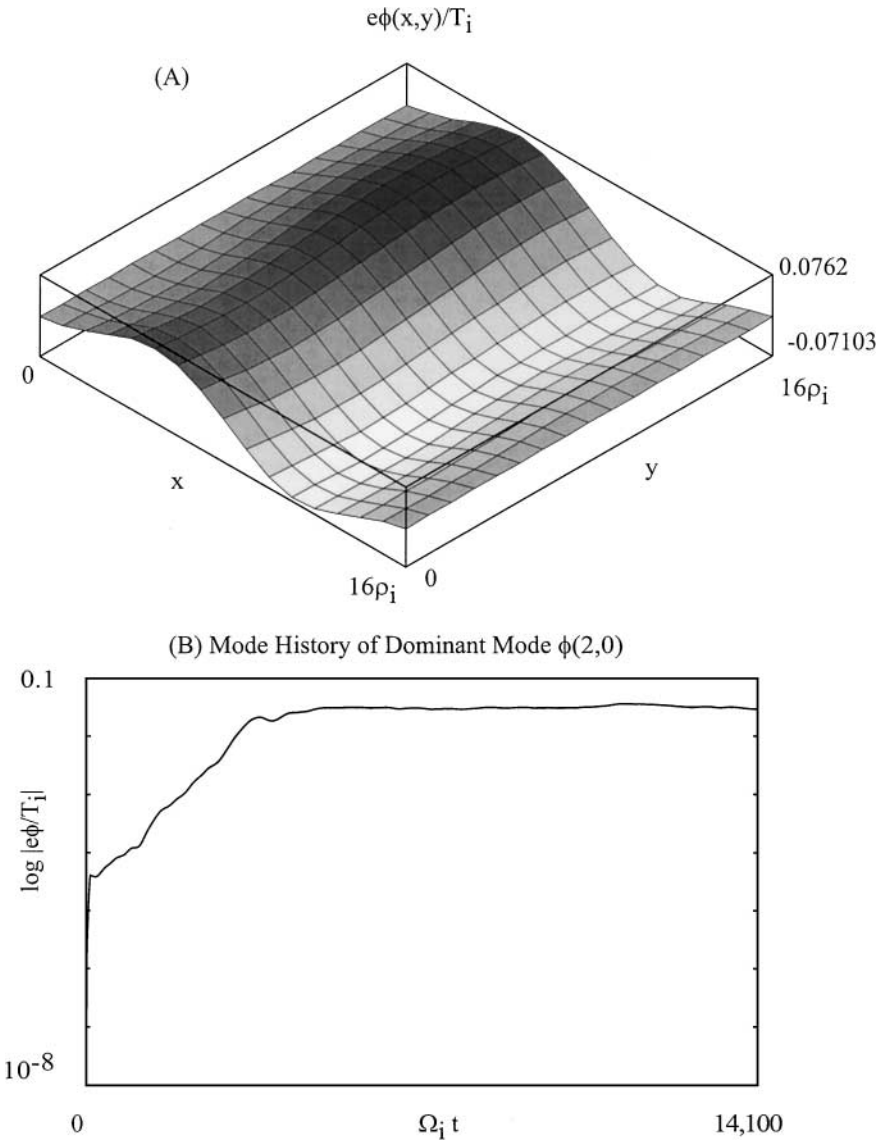

FIG. 3. Results using linear interpolation. (A) Surface plot of the electrostatic potential in the final nonlinear saturated state. Note the dominance of the fundamental zonal flow mode mode $\phi(k_x = 2\pi/L_x, k_y = 0)$. (B) The time evolution of the amplitude of the $\phi(k_x = 2\pi/L_x, k_y = 0)$ mode.

to be high because the self-generated shear flow is also stabilizing and therefore will tend to cause saturation at a lower level. This is indeed what is observed at later times, where the saturation level drops to approximately 0.03%. It is interesting that the initial saturation level is rather high, which implies that the initial (transient) saturation is dominated by $E \times B$ trapping and not the zonal flow shear stabilization. In addition, there is only a factor of two reduction in the saturation level at later times. This is in contrast to three-dimensional flux-tube simulations where zonal flow generation is the dominant saturation mechanism [24]. However, the two-dimensional bounded slab model is consistent with small global simulations which show a weaker effect of zonal flows on the saturation of the

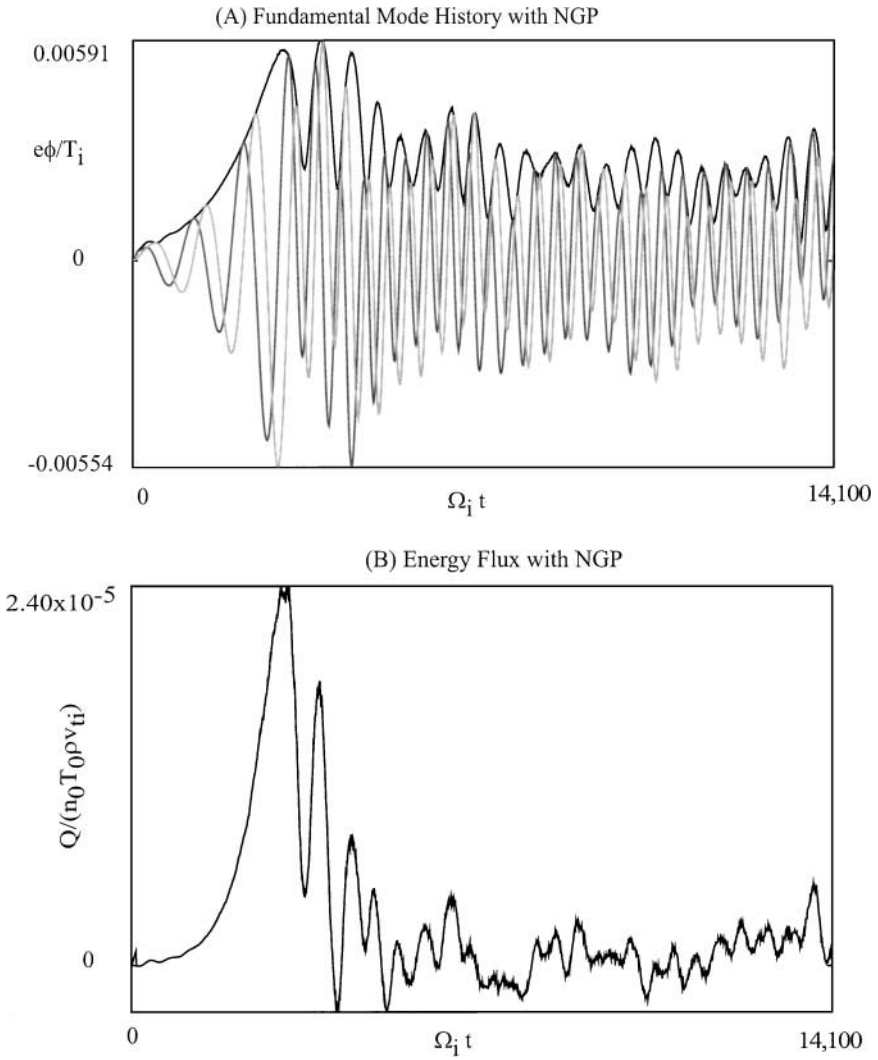

FIG. 4. Results similar to those shown in Fig. 1 except using NGP interpolation. There is little difference between NGP and linear interpolation. (A) Time evolution of the most unstable mode, $\phi(k_x = \pi/L_x, k_y = 2\pi/L_y)$; (B) the nonlinear ion energy flux.

turbulence and show a coherent $\phi(2, 0)$ zonal flow [25, 26]. This simple two-dimensional shearless slab model has the minimal physics for the generation of a zonal flow mode and ensuing nonlinear saturation and shows qualitative features which are similar to small three-dimensional toroidal global simulations. The limitation of this model is the fact that it is very coherent, whereas three-dimensional simulations are more turbulent, with many interacting modes.

4. FINITE-SIZE PARTICLE EFFECTS WITH GYROAVERAGING

For simplicity, we restrict our discussion to the model discussed above in Sections 2 and 3. In addition, we analyze interpolations in the two directions perpendicular to the magnetic

field and ignore interpolation parallel to the magnetic field, which is unaffected by the gyroaveraging procedure.

Numerical interpolation from grid to particles effects the response of δf through Eq. (1), and interpolation from the particles to the grid affects the field equations through Eq. (2). For example, let us examine how the gyroaveraged guiding center perturbed ion density $\delta\bar{n}_i$ in Eq. (2) is numerically calculated by taking into account the effect of using finite-size particles [13]. In Fourier space

$$\delta\bar{n}_i(\mathbf{k}) = \int J_0[k_\perp \rho(\mu)]\delta f(\mathbf{k}, v_{||}, \mu)\, dv_{||}\, B d\mu, \tag{6}$$

where $\delta n_i(\mathbf{k})$ is the guiding center (not gyroaveraged) density. Numerically, the grid interpolation of this quantity is approximated using both the four-point gyroaverage and a particle interpolation scheme, so that

$$\delta\bar{n}_i^{Num}(\mathbf{k}) = \int \tilde{S}_n^M[\mathbf{k}, \boldsymbol{\Delta}\mathbf{x}, \rho(\mu)]\delta f(\mathbf{k}, v_{||}, \mu)\, dv_{||}\, B d\mu, \tag{7}$$

where $\delta\bar{n}_i^{Num}$ is the numerical approximation to $\delta\bar{n}_i$ and $\tilde{S}_n^M$ is an interpolation function that is explained in detail below. Here, we attempt to analyze the interpolation scheme by using the finite-size particle shape function $S(\mathbf{x})$ [13]. We assume $S(\mathbf{x})$ to be separable and to have the same functional dependence in all directions. For example in two dimensions $S(x, y) = S(x)S(y)$. Therefore, we only need to specify the one-dimensional shape function $S(u) = S(u, \Delta u)$, where u is a dummy variable and could be equal to x or y with Δu the corresponding grid size Δx or Δy. For NGP interpolation $S = S_0$, where the subscript indicates the order of the interpolation scheme,

$$S_0(x) = \frac{1}{\Delta x}\begin{cases} 1 & \text{for } |x| \le \Delta x/2, \\ 0 & \text{otherwise.} \end{cases} \tag{8}$$

For linear interpolation $S = S_1$,

$$S_1(x) = \frac{1}{\Delta x}\begin{cases} 1 - \frac{|x|}{\Delta x} & \text{for } |x| \le \Delta x, \\ 0 & \text{otherwise.} \end{cases} \tag{9}$$

We call these "bare" numerical interpolation functions because they do not include the numerical gyroaveraging process [7]. The shape affects both the field interpolation to the particles, thereby modifying the gyrokinetic Vlasov equation, Eq. (1), and the deposition of the ion density, thereby modifying Eq. (2). The kinetic theory with finite-size particles can be carried through in various simple limits (see Ref. [13]) and one result is that the linear theory is modified to be $(\omega')^2 = S^2(\mathbf{k})\omega^2$, where ω' is the frequency rate of the finite-size particle plasma.

Gyroaveraging is accomplished by averaging M points on a ring [7]. This can be written

$$\tilde{S}_n^M(\mathbf{x}) \equiv \frac{1}{M}\sum_{m=0}^{M-1} S_n\left[x + \rho\cos\left(\frac{2\pi m}{M}\right)\right] S_n\left[y + \rho\sin\left(\frac{2\pi m}{M}\right)\right], \tag{10}$$

where $\rho = \rho(\mu)$ is a function of the individual particle's magnetic moment $\mu = \frac{mv_\perp^2}{2B}$ and the $\boldsymbol{\Delta}\mathbf{x}$ dependence will no longer be written explicitly. The subscript n identifies the order

of the interpolation scheme, as in Eqs. (8)–(9), and the superscript M identifies the number of points taken in the gyroaverage about the circular ring. We write $\tilde{S}(\mathbf{x})$ to emphasize that this shape function includes the gyroaveraging over points on a ring. We now Fourier transform $\tilde{S}(\mathbf{x})$ to see its effect in Fourier space using $\tilde{S}(\mathbf{k}) = \frac{1}{\sqrt{2\pi}} \int S(\mathbf{x}) e^{i\mathbf{k}\cdot\mathbf{x}}\, d\mathbf{x}$, obtaining

$$\tilde{S}_n^M(\mathbf{k}) = S_n(k_x) S_n(k_y) \left\{ \frac{1}{M} \sum_{m=0}^{M-1} \exp\left[i k_x \rho \cos\left(\frac{2\pi m}{M} \right) \right] + \exp\left[i k_y \rho \sin\left(\frac{2\pi m}{M} \right) \right] \right\} \quad (11)$$

for the gyroaverage about the circular ring. We define the quantity in the brackets as $\tilde{J}_0^M \equiv \{\cdots\}$, where $\tilde{J}_0$ is the numerical approximation to $J_0(k_\perp \rho_i)$, with the zero-order Bessel function appearing in the gyrokinetic equations. For the most typical choice of M, $M = 4$, $\tilde{J}_0^4$ simply reduces to

$$\tilde{J}_0^4 = \frac{1}{2}[\cos(k_x \rho) + \cos(k_y \rho)]. \quad (12)$$

The main point here is that the gyroaverage can be cast as a particle-shape function in a way similar to the interpolation function in PIC simulation. This means that the gyroaveraging produces smoothing or smearing of the particle charge density over nearby cells. Therefore, the bare particle-shape function can be low order and does not produce much effect in the simulation results.

Figure 5 shows $\tilde{S}_0^4$ as a function of $k_x \Delta x$ and $k_y \Delta y$ with $\rho = \Delta x = \Delta y$, which is a typical choice of parameters in large-scale gyrokinetic simulations of ITG turbulence. We note that different particles have different gyroradii. We choose $\rho = \Delta x = \Delta y$ for illustration purposes only. For small $k_\perp \rho$ this plot looks similar to $J_0(k_\perp \rho)$ (which is not shown).

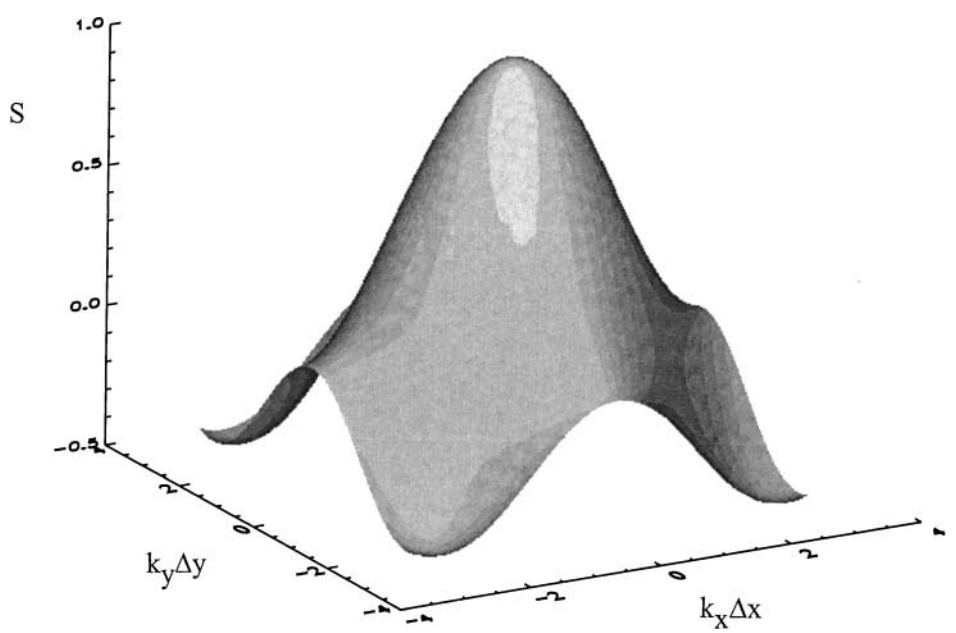

FIG. 5. A two-dimensional plot of $\tilde{S}_0^4(k_x \Delta x, k_y \Delta y)$. There is an azimuthal asymmetry in this function for $k_\perp \rho \gtrsim 1$ which is not found for $J_0(k_\perp \rho)$.

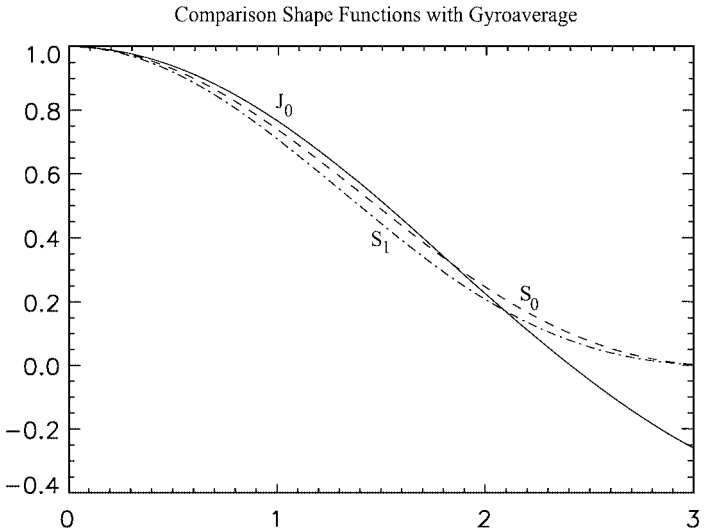

FIG. 6. Comparison of $\tilde{S}_0^4$ (dashed line), $\tilde{S}_1^4$ (dashed–dotted line), and J_0 (solid line) as a function of $k_x\Delta x$ with $k_y\Delta y = 0$ and $\rho = \Delta x$. There is little difference between them for $k_\perp\rho \lesssim 1$.

However, for larger $k_\perp\rho$ asymmetries exist in the numerical function (Fig. 5) which are not present in $J_0(k_\perp\rho)$, which corresponds to numerical error in the numerical gyroaverage. Figure 6 compares $\tilde{S}_1^4$ and $\tilde{S}_0^4$ as a function of $k_x\Delta x$ with $k_y\Delta y = 0$, showing that for $k_x\Delta x \lesssim 1$ there is little difference between the two. $k_y\Delta y$ is set to zero in Fig. 6. $J_0(k_\perp\rho)$ is also shown in Fig. 6 for comparison with $\rho = \Delta x = \Delta y$. Figure 7 compares the bare particle shape S_0 and S_1 along with J_0 as a function of $k_x\Delta x$ with $k_y\Delta x = 0$. $\rho = \Delta x$ is taken when plotting $J_0(k_\perp\rho)$ in Fig. 7. When the bare shape functions (with no gyroaveraging)

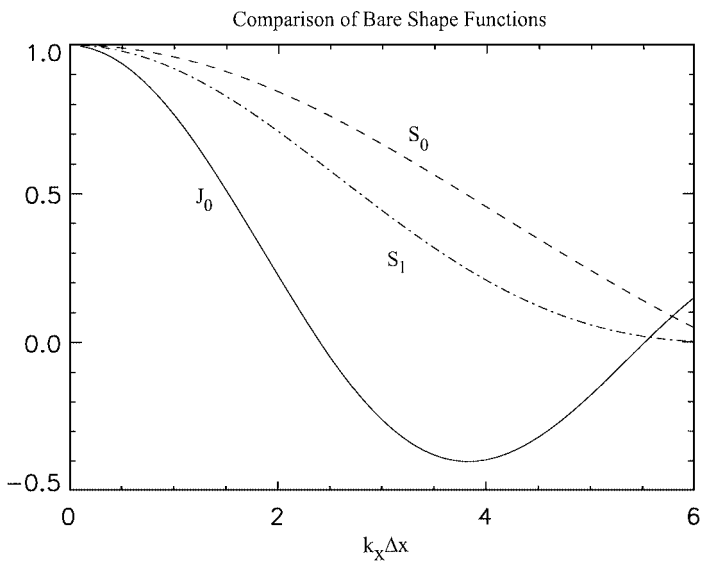

FIG. 7. Comparison of the bare particle-shape functions S_0 (dashed line) and S_1 (dashed–dotted line) along with J_0 (solid line) as a function of $k_x\Delta x$ with $k_y\Delta x = 0$. There is much more difference between these functions. $\rho = \Delta x$ is taken when plotting $J_0(k_\perp\rho)$.

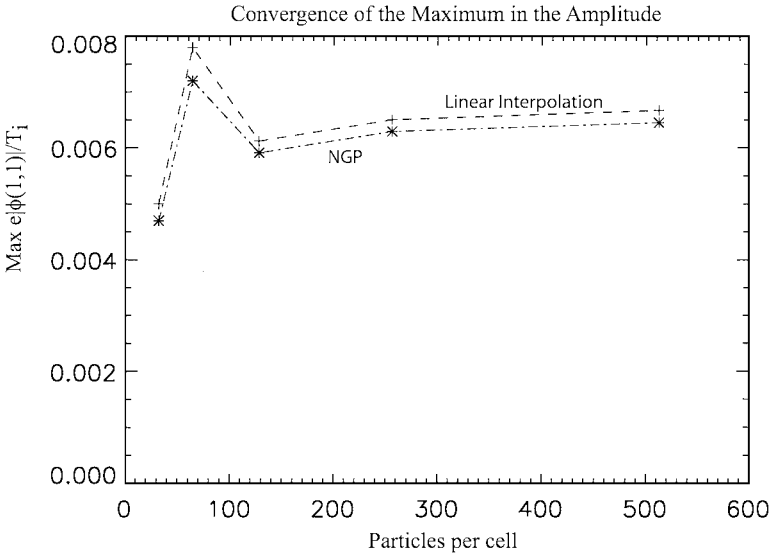

FIG. 8. Convergence with respect to particle number for the peak value of the amplitude of the most unstable mode, $\phi(k_x = \pi/L_x, k_y = 2\pi/L_y)$. This is a transient quantity and extremely sensitive to particle number. The dashed line is NGP interpolation and the dashed–dotted line is linear interpolation.

are compared, there is much more of a difference at larger $k_\perp \Delta x$, which may explain larger differences between NGP and linear interpolation in conventional PIC simulation (without any gyroaveraging). In this paper, only gyrokinetic simulation has been used and good agreement between NGP and linear interpolation is found with little difference in the convergence properties with respect to particle number.

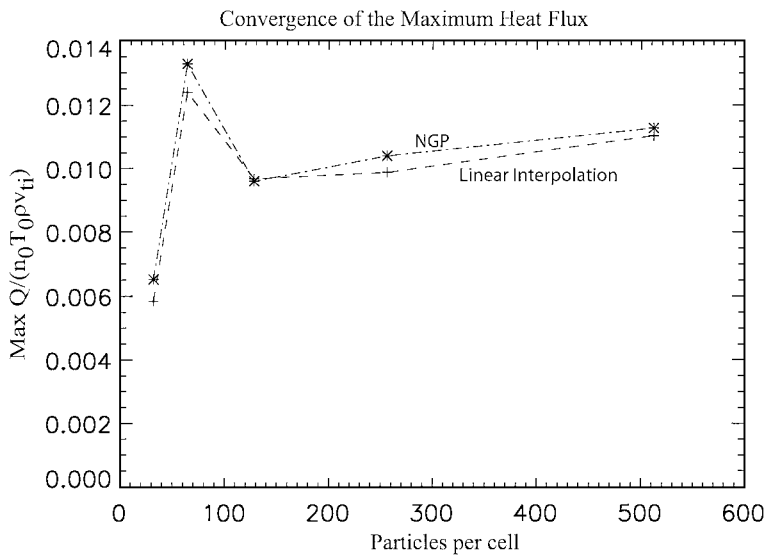

FIG. 9. Convergence with respect to particle number of the peak value of χ_i, the ion heat diffusivity. This is a transient quantity and extremely sensitive to particle number. The dashed line is NGP interpolation and the dashed–dotted line is linear interpolation.

Figures 8 and 9 show convergence with respect to particle number for the peak value of the most unstable mode amplitude and energy flux, respectively. The dashed line is linear interpolation and the dashed–dotted line is NGP interpolation. Both of these quantities are transient quantities and are extremely sensitive to particle number. Note that the two lines track each other fairly well and converge at what appears to be the same rate. There are slight differences between the converged results ($<10\%$). These differences are typically not taken as significant in tokamak turbulence and transport calculations. Similar convergence of the saturated turbulence is found in a more complex three-dimensional toroidal flux-tube simulation in Ref. [14]. Figure 1, which was previously published in Ref. [14], shows particle number convergence for both NGP and linear interpolation of the ion heat diffusivity and the field energy (see Ref. [14] for further details and the parameters used).

5. SUMMARY

Large-scale gyrokinetic particle simulations have used NGP interpolation, producing converged results at much faster speeds (see, for example, Ref. [14] and Fig. 1). In the perpendicular plane, NGP involves one gather/scatter of a grid quantity, whereas linear interpolation involves four. The overall number of gathers/scatters is increased by a factor of four in gyrokinetic simulation because of the four-point gyroaverage. We conclude that the reason that NGP works so well is that the numerical gyroaverage can be viewed as a finite particle shape which masks the underlying bare particle-shape function. This is true for ions with gyroaveraging and when the perpendicular grid size is on the scale of the ion gyroradius. For simulations using drift-kinetic electrons, there is no reason to expect NGP to perform as well. A simple two-dimensional slab gyrokinetic simulation model of zonal flow generation and nonlinear saturation was presented and used to test the interpolation schemes. The limitation of this model is that it is dominated by a small number of modes whereas three-dimensional simulations exhibit broadband turbulence. It does, however, show the generation of the zonal flow, and initial saturation, in its simplest form. This simulation model showed that convergence with respect to particle number is virtually identical for NGP and linear interpolation. Similar results are found in three-dimensional toroidal gyrokinetic simulations [14].

ACKNOWLEDGMENTS

Thanks to Charlson Kim, University of Colorado, Boulder, and Lester Chen, Harvard University, for helpful discussions. This work is supported by the Department of Energy and is part of DOE's Plasma Microturbulence Project.

REFERENCES

1. S. E. Parker, W. W. Lee, and R. Santoro, Gyrokinetic simulation of ion temperature gradient driven turbulence in 3D toroidal geometry, *Phys. Rev. Lett.* **71**, 2042 (1993).
2. M. Dimits, T. J. Williams, J. A. Byers, and B. I. Cohen, Scalings of ion-temperature-gradient-driven anomalous transport in tokamaks, *Phys. Rev. Lett.* **77**, 71 (1996).
3. R. D. Sydora, V. K. Decyk, and J. M. Dawson, Fluctuation-induced heat transport results from a large global 3D toroidal particle simulation model, *Plasma Phys. Control. Fusion* **38**, A281 (1996).
4. Z. Lin, T. S. Hahm, W. W. Lee, W. M. Tang, and R. B. White, Turbulent transport reduction by zonal flows: Massively parallel simulations, *Science* **281**, 1835 (1998).

5. W. Dorland, F. Jenko, M. Kotchenreuther, and B. Rogers, Electron temperature gradient driven turbulence, *Phys. Rev. Lett.*, **85**, (26), 5579 (2000).
6. W. W. Lee, Gyrokinetic approach in particle simulation, *Phys. Fluids* **26**, 556 (1983).
7. W. W. Lee, Gyrokinetic particle simulation model, *J. Comput. Phys.* **72**, 243 (1987).
8. A. Dimits and W. W. Lee, Partially linearized algorithms in gyrokinetic particle simulation, *J. Comput. Phys.* **107**(2), 309 (1993).
9. S. E. Parker and W. W. Lee, A fully nonlinear characteristic method for gyrokinetic simulation, *Phys. Fluids B* **5**, 77 (1993).
10. G. Hu and J. A. Krommes, Generalized weighting scheme for delta f particle-simulation method, *Phys. Plasmas* **1**, 863 (1994).
11. A. Langdon and C. K. Birdsall, Theory of plasma simulation using finite-size particles, *Phys. Fluids* **13**, 2115 (1970).
12. W. Kruer, J. Dawson, and B. Rosen, The dipole expansion method for plasma simulation, *J. Comput. Phys.* **13**, 114 (1973).
13. C. Birdsall and A. B. Langdon, *Plasma Physics Via Computer Simulation* (McGraw–Hill, New York, 1985).
14. C. Kim and S. E. Parker, Massively-parallel three-dimensional toroidal gyrokinetic flux-tube turbulence simulation, *J. Comput. Phys.* **161**(2), 589 (2000).
15. F. L. Hinton and M. N. Rosenbluth, Dynamics of axisymmetric E × B and poloidal flows in tokamaks, *Plasma Phys. Control. Fusion* **41**, A653 (1999).
16. Z. Lin, T. S. Hahm, W. W. Lee, W. M. Tang, and P. H. Diamond, Effects of collisional zonal flow damping on turbulent transport, *Phys. Rev. Lett.* **83**, 3645 (1999).
17. B. Rogers, W. Dorland, and M. Kotschenreuther, Generation and stability of zonal flows in ion-temperature gradient mode turbulence, *Phys. Rev. Lett.* **85**, 5336 (2000).
18. W. Dorland and G. W. Hammett, Gyrofluid turbulence models with kinetic effects, *Phys. Fluids B* **5**, 812 (1993).
19. G. W. Hammett, M. A. Beer, W. Dorland, S. C. Cowley, and S. A. Smith, Developments in the gyrofluid approach to Tokamak turbulence simulations, *Plasma Phys. Control. Fusion* **35**, 973 (1993).
20. M. A. Beer, S. C. Cowley, and G. W. Hammett, Field-aligned coordinates for nonlinear simulations of tokamak turbulence, *Phys. Plasmas* **2**, 2686 (1995).
21. W. W. Lee and W. M. Tang, Gyrokinetic particle simulation of ion temperature gradient drift instabilities, *Phys. Fluids* **31**, 612 (1988).
22. S. E. Parker, W. Dorland, R. A. Santoro, M. A. Beer, Q. P. Liu, W. W. Lee, and G. W. Hammett, Comparisons of gyrofluid and gyrokinetic simulations, *Phys. Plasmas* **1**, 1461 (1994).
23. N. Mattor and S. E. Parker, Nonlinear kinetic fluid equations, *Phys. Rev. Lett.* **79**, 3419 (1997).
24. A. M. Dimits, G. Bateman, M. A. Beer, B. I. Cohen, W. Dorland, G. W. Hammett, C. C. Kim, J. E. Kinsey, M. Kotschenreuther, A. H. Kritz, L. L. Lao, J. Mandrekas, W. M. Nevins, S. E. Parker, A. J. Redd, D. E. Shumaker, R. Sydora, and J. Weiland, Comparisons and physics basis of tokamak transport models and turbulence simulations, *Phys. Plasmas* **7**, 969 (2000).
25. J. C. Cummings, "*Gyrokinetic Simulation of Finite-Beta and Self-Generated Sheared-Flow Effects on Pressure-Gradient-Driven Instabilities*," Ph.D. thesis, (Princeton University, Princeton, NJ, 1995).
26. S. E. Parker, C. Kim, and Y. Chen, Large-scale gyrokinetic turbulence simulations: Effects of profile variation, *Phys. Plasmas* **6**, 1709 (1999).